The Journal of Green Energy and Environmental Engineering

Research Paper

Pyrolytic Oil Based Drilling Cuttings/Orange Peel Biochar for Passivation and Remediation of Copper Lead Contaminated Soil

Omar Farooq[1,*], Tariq Jameel[2]

[1] Department of Chemical Engineering, Eastern Michigan University, Ypsilanti, Michigan, USA
[2] School of Life Science, Universityof Wollongong, Wollongong, New SouthWales, Australia
*Corresponding author: OCFarooq@emich.edu; tJameel@uow.edu.au

Abstract. An 83-day passivation and remediation experiment was conducted by incorporating pyrolytic oil-based drilling cuttings (OBDC)/orange peel (OB) biochar (OBDCs-OB) into soil co-contaminated with Cu(II) and Pb(II). The study systematically investigated the passivation efficiency of OBDCs-OB on copper-lead contaminated soil and its subsequent influence on soil microbial communities. Results demonstrated that OBDCs-OB possessed abundant surface functional groups including hydroxyl (–OH) and carboxyl (–COOH), mineral constituents such as carbonate rocks and clay minerals, and a well-developed porous architecture, all of which rendered it a highly effective adsorbent. Compared with untreated blank soil, the cation exchange capacity (CEC) of OBDCs-OB-amended soil increased substantially by 18.29 cmol/kg, while the pH was stably maintained at 6.80 throughout the experimental period. Furthermore, the acid-soluble fractions of Cu(II) and Pb(II) in the soil decreased by 18.21% and 20.07%, respectively, and the potential leaching toxicity of copper and lead was reduced by 52.8% and 92.8%, unequivocally confirming the effective passivation of both heavy metals. Concurrently, the maximum soil microbial population reached 8.6×10^{10} cfu/g, and peak activities of dehydrogenase and urease were recorded at 127.10 μg·TPE/(g·6 h) and 167.10 mg·NH_3-N/(kg·24 h), respectively, indicating a marked enhancement in microbial community diversity, richness, and overall growth promotion.

Keywords: *pyrolytic oil based drilling cuttings; heavy metal ion immobilization; copper; lead; microbial community structure; soil remediation; environmental protection*

Received on 02 March 2026, Accepted on 05 June 2026, Published on 07 July 2026

1 Introduction

Typically, Cu(II) and Pb(II) coexist in contaminated soils and infiltrate into the soil matrix through rainwater leaching and surface runoff[1-2], which not only diminishes crop yields and degrades surrounding aquatic ecosystems but also poses protracted risks to ecological integrity and human health[3]. Current remediation strategies for heavy metal-contaminated soils[4] encompass physical, chemical, biological, and integrated approaches, including soil replacement, chemical leaching, in-situ chemical passivation, phytoremediation, microbial remediation, and combined chemical-biological techniques. Among these, in-situ chemical passivation has gained widespread adoption owing to its economic viability, operational convenience, and rapid efficacy[5]. Biochar, benefiting from diverse feedstock availability and superior physicochemical properties, has emerged as a prevalent chemical passivator for heavy metal remediation, with common waste-derived precursors such as corn cobs and orange peel (OB)[6]. Additionally, clay mineral-based materials like kaolin can also serve as effective passivating agents[7-8]. Given the low cost and abundant supply of waste materials, their conversion into value-added products through low-cost treatment aligns with the principles of waste minimization, harmlessness, and resource recovery.

During shale gas extraction, massive quantities of oil-based drilling cuttings (OBDC) are generated, containing diverse hazardous organic and inorganic constituents including petroleum hydrocarbons and heavy metals. Untreated OBDC is classified as hazardous waste and is subject to strict regulations prohibiting arbitrary transfer

or disposal[9]. Recent studies have demonstrated that pyrolytic treatment of OBDC enables both oil recovery and secondary utilization of the solid residue[9]. The pyrolysis process drives off organic matter, volatilizes moisture and light oils, and cracks heavy oils into gas, liquid, and solid phases; the solid fraction consists predominantly of drilling cuttings residue with minimal residual organics[10], forming a carbon-rich slag that exhibits considerable promise as an adsorbent material[11]. LIU et al.[12] employed pyrolytically derived OBDC carbon to adsorb Pb(II), Cr(VI), and Cu(II) from aqueous solutions, reporting adsorption capacities superior to those of commercial coconut-shell activated carbon; however, its application in soil remediation remains limited. Direct incorporation of untreated OBDC into acidic soils does not induce heavy metal exceedance, and increasing OBDC dosages promote dissolution of carbonate minerals, thereby elevating soil pH[13] and ameliorating soil physicochemical properties. Concurrently, its distinctive physicochemical composition facilitates heavy metal immobilization, underscoring the latent potential of pyrolyzed OBDC residues for passivating heavy metals in contaminated soils. Nevertheless, the fine particle size of pyrolyzed OBDC residues renders them prone to agglomeration, which compromises performance; consequently, waste OB was adopted as a carrier for co-pyrolysis to enhance overall efficacy.

Existing soil passivation studies predominantly emphasize the immobilization efficiency of amendments on heavy metals, with scant attention paid to their impact on soil microbial activity. Hence, this work integrated OBDC with plant-derived pyrolytic biochar to bolster biocompatibility[14-15]. Utilizing OB waste and OBDC sourced from Sichuan Province, pyrolytic OBDC/OB biochar (OBDCs-OB) was synthesized. The study comprehensively evaluated the influence of OBDCs-OB on soil physicochemical properties, heavy metal passivation efficiency, and microbial community dynamics during the remediation of copper-lead co-contaminated soil, thereby projecting the application prospects of pyrolytic OBDC in this context.

2 Experimental Part

2.1 Reagents, Materials and Instruments

OBDC was procured from Well H1 of the Weiyuan shale gas field. OB was obtained from Cisidou. $Cu(NO_3)_2$, $Pb(NO_3)_2$, $BaCl_2$, NaOH, NaCl, toluene, urea, and citric acid (analytical reagent grade) were supplied by Cidou Kelong Chemical Reagent Factory. Beef extract and peptone (biochemical reagents) were purchased from OAOID Co., Ltd., USA. Key instrumentation included a SK-G06123K vacuum tube furnace (Tilead Electric Furnace Co., Ltd.), a WQF-520 Fourier transform infrared spectrometer (Beijing Ruili Analytical Instrument Co., Ltd.), an X'Pert PRO MPD X-ray powder diffractometer (PANalytical, Netherlands), a Zeiss Supra55 scanning electron microscope (Zeiss, Germany), and an APSP2460 automatic specific surface area and pore size analyzer (Micromeritics Instrument Corporation, USA).

The baseline soil was collected from the top 10–20 cm layer at the third phase campus of Southwest Petroleum University, Chengdu, Sichuan (30°83'16"N, 104°19'04"E). Baseline physicochemical parameters were: pH 7.52±0.02, moisture content 17.30%, available nitrogen (AHP) 300.00 mg/kg, available phosphorus (AP) 129.26 mg/kg, and total organic carbon (TOC) 2.13 wt%. Contaminated soil was prepared by air-drying the baseline soil, sieving through a 2 mm mesh, and spiking each kilogram with 2.3500 g $Cu(NO_3)_2$ and 1.5985 g $Pb(NO_3)_2$, yielding nominal Cu(II) and Pb(II) concentrations of approximately 800 and 1000 mg/kg[16], roughly fourfold the thresholds stipulated in GB 15618-2018 "Soil Environmental Quality Standard for Agricultural Land in China". The homogenized soil was equilibrated at 25 °C for three months to allow heavy metal stabilization.

2.2 Preparation and Characterization of Adsorbent

Preliminary optimization identified the optimal mass ratio of OBDC to OB as 1:1[17]. Accordingly, 10 g OBDC was dispersed in 500 mL deionized water under stirring for 30 min, followed by addition of 10 g OB (pre-dried at 80 °C for 24 h and sieved through 2 mm). Stirring continued for 2 h, after which the slurry was filtered and oven-dried at 80 °C for 24 h. The dried mixture was pyrolyzed in a vacuum tube furnace at 500 °C (heating rate 20 °C/min) for 30 min, then cooled to 25 °C. The resulting product was rinsed thrice with deionized water and dried at 80 °C for 24 h[18] to yield OBDCs-OB. Single-component controls—OBDC-derived biochar (OBDCs) and OB-derived biochar (OBs)—were prepared via identical pyrolysis protocols[17].

2.3 Soil Remediation Experiment

A total of 2500 g contaminated soil was partitioned into five equal 500 g aliquots. One aliquot received no amendment and served as the blank control (C0). The remaining four were supplemented with: 5.0 wt% nutrient mixture (comprising 94.4% glucose, 4.7% NH_4Cl, and 0.9% KH_2PO_4 by mass); 5.0% nutrients + 5.0% OBs; 5.0% nutrients + 5.0% OBDCs; and 5.0% nutrients + 5.0% OBDCs-OB. Soil mass was proportionally reduced to maintain a constant total of 500 g per treatment. Each mixture was placed in a plastic flowerpot[19], labeled C1–C4, and subjected to three parallel replicates. Incubation proceeded at 25 °C for 83 days, with soils turned every two days. Periodic sampling assessed CEC, pH, heavy metal speciation, microbial activity, and community structure. Nutrients were incorporated to sustain essential microbial metabolic functions.

2.4 Characterization and Performance Tests

2.4.1 Soil CEC and pH Determination

CEC was quantified by the $BaCl_2$-NaOH titration method[20]. Soil pH was measured in accordance with HJ 962-2018 "Determination of Soil pH—Potentiometric Method".

2.4.2 Extraction and Determination of Soil Heavy Metal Ions

Heavy metal speciation was resolved by the BCR sequential extraction procedure[21], partitioning metals into acid-soluble (F1), reducible (F2), oxidizable (F3), and residual (F4) fractions. Potential leaching toxicity was evaluated using the toxicity characteristic leaching procedure (TCLP)[22].

2.4.3 Soil Microbial Activity and Community Structure Analysis

On days 0, 7, 14, 21, 28, 35, 49, 63, and 83, 4 g soil was suspended in 20 mL sterile centrifuge tubes with 10 mL sterile deionized water, vortexed for 5 min, and 1 mL supernatant was serially diluted tenfold into 9 mL liquid microbial medium across seven gradients (triplicate). Cultures were incubated at 37 °C for 48 h, and total bacterial counts were derived via the most probable number (MPN) method[23]. Medium composition: 3 g/L beef extract, 5 g/L peptone, 5 g/L NaCl, pH adjusted to ~7.0 with 0.1 mol/L NaOH, autoclaved at 121 °C for 20 min (9 mL per vial). On days 0, 7, 14, 28, 35, 41, 49, 56, 63, 73, and 83, dehydrogenase activity was determined by the TTC reduction method (ISO 23753-1:2019), with TPE denoting triphenylformazan, and urease activity by the sodium phenolate-sodium hypochlorite method (T/NAIA 011-2020). On days 0, 21, and 83, soil DNA was extracted for 16S rDNA amplicon sequencing[24]; libraries were constructed with indexed primers and sequenced on an Illumina NovaSeq platform, followed by offline bioinformatic analysis.

3 Results and Discussion

3.1 Material Characterization and Adsorption Performance

The proximate composition of raw OBDC was: organic matter (including total petroleum hydrocarbons) 8.10 wt%, gases (H_2, CH_4, CO) 2.70 wt%, moisture 4.12 wt%, and solid ash 85.08 wt%. Post-pyrolysis, organics, moisture, and gases were expelled, leaving merely 0.1% solid residue. Figure 1a presents FTIR spectra of OBs, OBDCs, and OBDCs-OB. A broad band at 3430 cm^{-1} was ascribed to surface –OH stretching, while the signal at 2928 cm^{-1} corresponded to aliphatic C–H vibrations. Peaks at 1608 and 1434 cm^{-1} were assigned to carbonyl C=O and ester/–COOH groups, respectively, and the 1100 cm^{-1} band indicated sulfate/silicate moieties[25]. The spectra confirmed that OBDCs-OB inherited vibrational signatures from both parent materials. Figure 1b displays XRD patterns: OBDCs comprised quartz (SiO_2), calcite ($CaCO_3$), pyrite (FeS_2), and clay minerals including muscovite ($KAl_2(AlSi_3O_{10})(OH)_2$) and kaolinite ($Al_2Si_2O_5(OH)_4$), consistent with the lithology of the Sichuan Longmaxi Formation shale[26]. OBDCs-OB diffractograms exhibited overlapping reflections from both OBs and OBDCs, verifying retention of inorganic phases.

DOI:

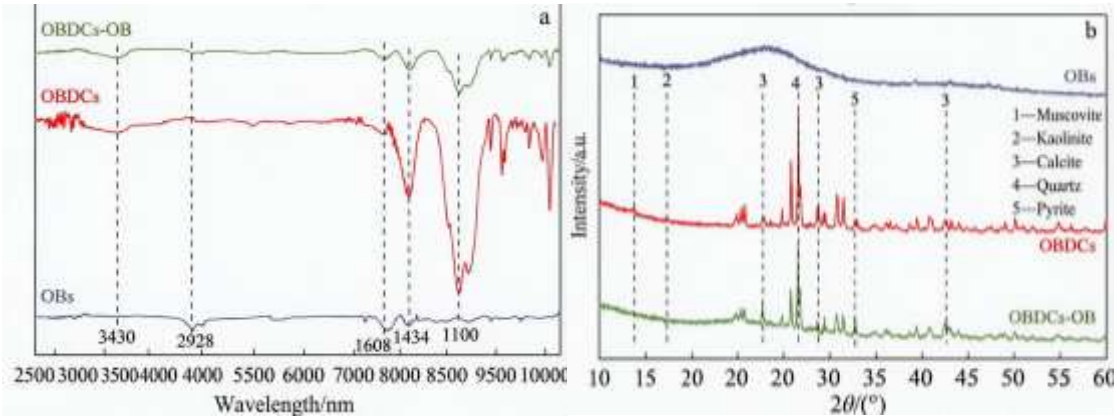

Figure 1 FTIR spectra (a) and XRD patterns (b) of OBs, OBDCs and OBDCs-OB

SEM micrographs (Fig. 2) revealed that OBs (Fig. 2a) possessed a porous, wrinkled morphology ideal for hosting OBDC pyrolysis ash. OBDCs (Fig. 2b) consisted of irregular, loosely layered particles. In OBDCs-OB (Fig. 2c), OBDCs adhered to OB pore walls and internal surfaces, generating a rough topography that furnished abundant adsorption sites and a high specific surface area conducive to Cu(II) and Pb(II) capture. N_2 adsorption-desorption isotherms and pore size distributions showed specific surface areas of OBDCs and OBDCs-OB at 8.44 and 7.73 m^2/g, far exceeding OBs' 0.72 m^2/g. Micropore volumes were 4.12×10^{-2} and 4.86×10^{-2} cm^3/g, respectively, versus 3.25×10^{-3} cm^3/g for OBs. Average pore diameters measured 18.14, 19.55, and 15.78 nm. Co-pyrolysis deposited OBDCs onto OB surfaces, reducing pore size while augmenting microporosity. The enlarged interfacial area facilitated contact between passivator and soil. Collectively, OBDCs-OB integrated –OH/–COOH functionality, carbonate/clay mineralogy, and hierarchical porosity, qualifying it as a versatile adsorbent. Prior work by the group[17] established maximum adsorption capacities for Cu(II) and Pb(II) at 95.11 and 164.08 mg/g in aqueous systems, obeying pseudo-second-order kinetics and Langmuir monolayer chemisorption.

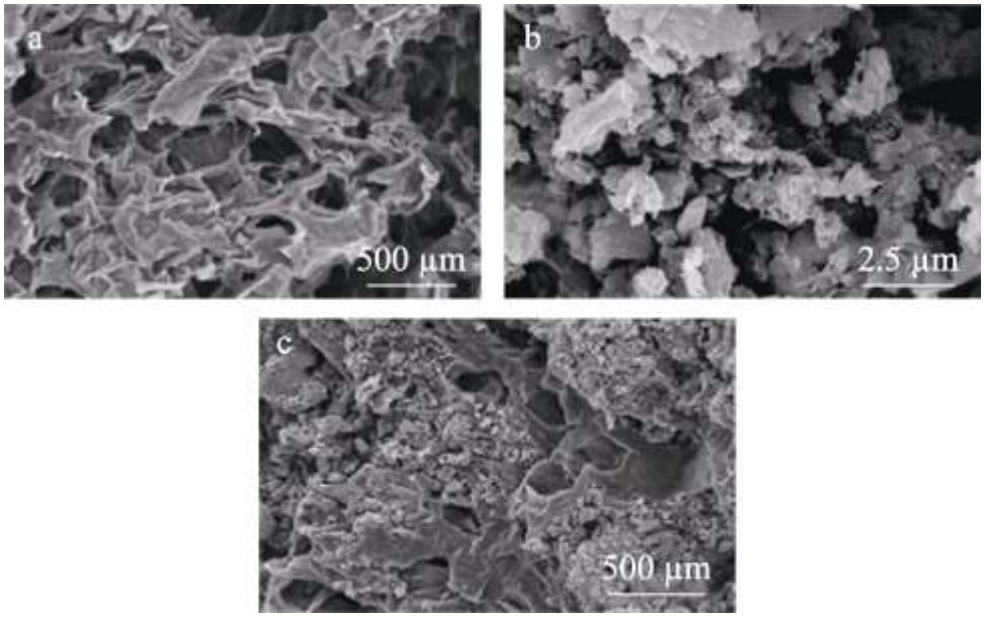

Figure 2 SEM images of OBs (a), OBDCs (b) and OBDCs-OB (c)

3.2 Soil CEC and pH Evolution

Figure 3a charts CEC dynamics post-amendment. All treatments except C0 and C1 enhanced CEC; increments for C2, C3, and C4 relative to baseline (85.11 cmol/kg) were 3.89, 12.94, and 18.29 cmol/kg, respectively. Surface –OH and –COOH groups complexed Cu(II)/Pb(II), while interlayer Na^+/K^+ in clay minerals exchanged with heavy

metal cations, elevating CEC[26]. OBDCs contributed more than OBs, and OBDCs-OB achieved the highest value by maximizing clay-soil contact. Although OBDCs-OB's specific surface area (7.73 m^2/g) marginally trailed OBDCs (8.44 m^2/g), co-pyrolysis suppressed OBDCs agglomeration, thus amplifying the CEC gain. Figure 3b depicts pH fluctuations. Initial pH values for C0–C4 were 7.52, 7.34, 7.22, 7.36, and 7.28. After 83 days, terminal pH values were 7.43, 6.90, 6.60, 7.12, and 6.80. Microbial metabolism acidified soils; OBs' inherent –COOH groups further favored acidophilic microbiota, accelerating pH decline. Conversely, carbonate minerals (calcite, dolomite) in OBDC constituted a natural buffer[26-27], with partial dissolution releasing CO_3^{2-} that hydrolyzed to yield OH^-, offsetting acidification proportionally to carbonate content.

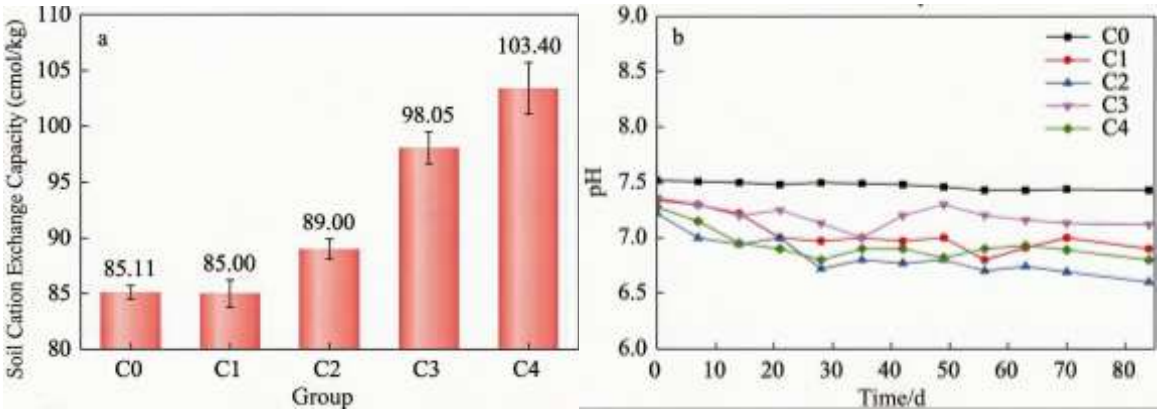

Figure 3 Change of CEC (a) and pH (b) of soil

3.3 Soil Heavy Metal Speciation

On day 83, BCR-extracted metal fractions (Fig. 4) showed that nutrient and biochar additions shifted speciation profiles: acid-soluble pools contracted while reducible, oxidizable, and residual fractions expanded. Relative to C0, acid-soluble Cu(II) in C1–C4 dropped by 6.01%, 11.61%, 13.50%, and 18.21%; acid-soluble Pb by 5.87%, 13.76%, 16.58%, and 20.07%. The residual fraction dominated over time, stabilizing both metals. Pb(II) exhibited a lower residual proportion than Cu(II), reflecting superior Pb passivation, interpretable by hard-soft acid-base theory: Pb(II) (hard acid) preferentially coordinates with –OH (hard base) over Cu^{2+} (soft acid)[16]. Elevated pH also promoted OH^--mediated precipitation, and clay interlayer cation exchange further sequestered metals.

Figure 5 quantifies potential leaching toxicity. C0 remained essentially unchanged, whereas all amendments reduced mobility. By day 83, C4 (OBDCs-OB) achieved reductions of 52.8% for Cu and 92.8% for Pb versus C0—the steepest declines among treatments. This directly correlated with diminished acid-soluble fractions (18.21% and 20.07% reductions). Passivator-metal interactions (complexation, ion exchange) curtailed leachable fractions[6], with Pb's lower acid-soluble baseline driving its dramatically lower toxicity.

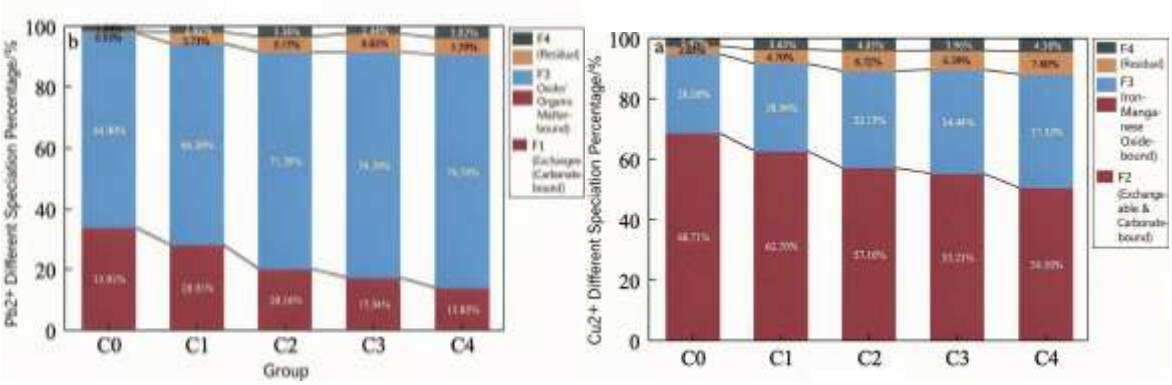

Figure 4 Morphological changes of Cu(Ⅱ) (a) and Pb(Ⅱ) (b) in soil during soil restoration

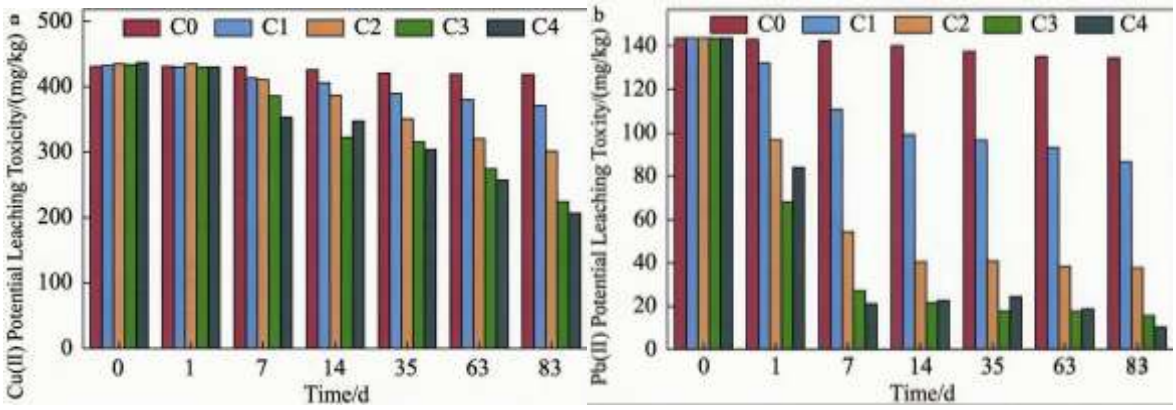

Figure 5 Potential leaching toxicity of Cu(Ⅱ) (a) and Pb(Ⅱ) (b) in soil

3.4 Soil Microbial Activity Dynamics

Microbial counts (Fig. 6) in all but C0 rose initially, peaked, then stabilized. OBDCs-OB (C4) attained a maximum of 8.6×10^{10} cfu/g on day 28, outperforming OBs (peak on day 21). Biochar's intrinsic biocompatibility fostered growth[14]. pH buffering by clay minerals and toxicity reduction co-operated to sustain a favorable microenvironment. Enzyme activities (Fig. 7) paralleled population trends: dehydrogenase and urease in C4 peaked at 127.10 μg·TPE/(g·6 h) and 167.10 mg·NH_3-N/(kg·24 h) on day 28. Alleviated metal stress coupled with biochar stimulation enhanced microbial vigor and enzymatic output[11]. OBs performed nearly as well as OBDCs-OB, confirming biochar's general stimulatory effect, while OBDCs deferred the activity maximum.

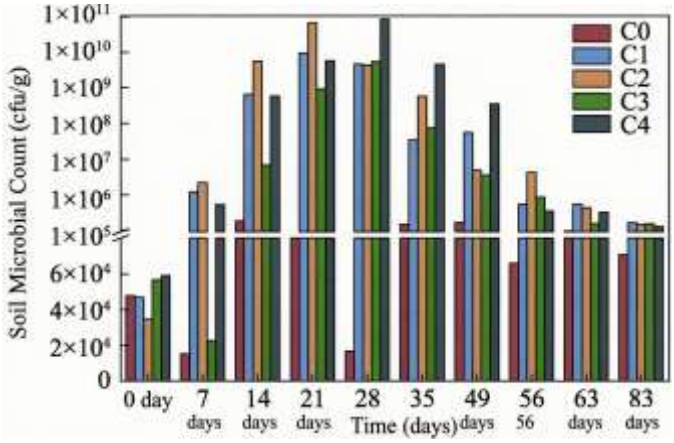

Figure 6 Change of soil microbial population

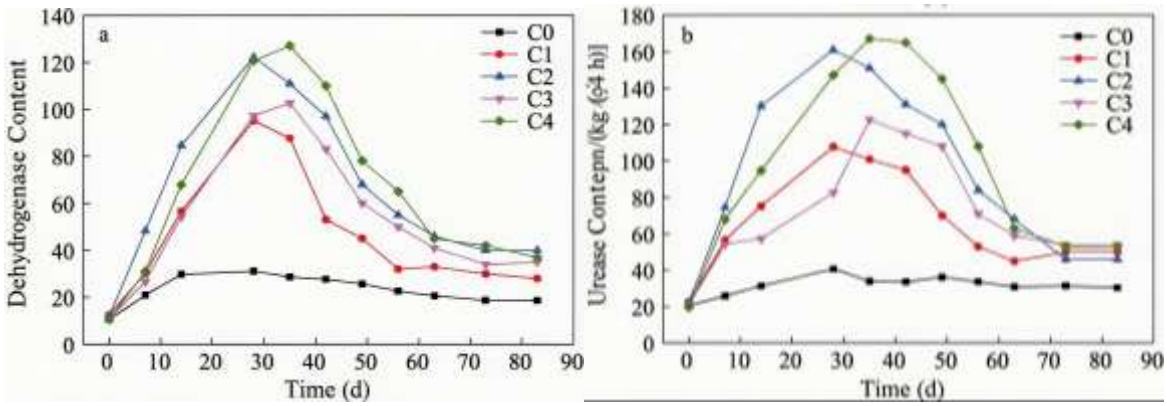

Figure 7 Change of dehydrogenase content (a) and urease content (b) in soil

DOI:

3.5 Soil Microbial Community Structure

Heavy metals reshape community composition. 16S rDNA sequencing yielded 589,894 valid sequences (414–427 bp). OTU clustering at 97% similarity produced 10,593 OTUs (Table 1). Day-21 OTU counts vastly exceeded day-83 counts, indicating higher early-stage richness. Diversity indices (Shannon, Chao1, ACE) were highest for C4 on both sampling days, confirming OBDCs-OB's superiority in augmenting diversity and richness. By day 83, indices declined across all groups, likely tracking reduced microbial loads and enzyme levels. Phylum-level relative abundance (Fig. 8) identified Proteobacteria, Actinobacteria, Firmicutes, and Acidobacteria as dominant on day 21; by day 83, only the first three persisted prominently. These taxa are documented heavy-metal-tolerant residents of polluted soils[31-34]. Microbial acclimation enriched resistant strains, yet C2–C4 did not markedly alter dominant phylum distribution versus C1, signifying that OBDCs-OB enhanced diversity without disrupting core community membership.

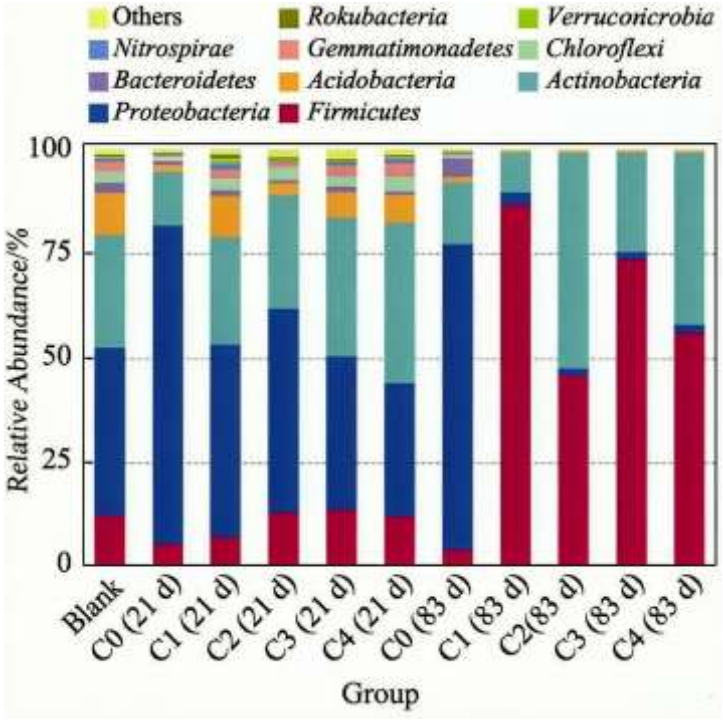

Figure 8 Bar diagrams of relative abundance of species at phylum level

The passivation and remediation of copper–lead co-contaminated soil by pyrolytic oil-based drilling cuttings/orange peel biochar composite (OBDCs-OB) operates through a hierarchically orchestrated, multi-stage mechanism that seamlessly integrates physical confinement, surface coordination chemistry, mineral-mediated ion exchange, carbonate alkalinity buffering, precipitate formation, and microbe-driven biogeochemical stabilization into a self-reinforcing cascade, such that each individual process amplifies the others rather than acting in isolation. At the foundational architectural level, co-pyrolysis of oil-based drilling cuttings (OBDC) and orange peel (OB) at 500°C under vacuum fuses the macroporous, highly wrinkled carbon scaffold derived from orange peel—which alone exhibits a negligible specific surface area of merely 0.72 m^2/g and a micropore volume of 3.25×10^{-3} cm^3/g—with the mineral-rich pyrolytic ash of drilling cuttings, producing a composite material (OBDCs-OB) possessing a specific surface area of 7.73 m^2/g and a micropore volume of 4.86×10^{-2} cm^3/g that far surpasses either parent component and approaches the textural properties of the OBDC-only biochar (8.44 m^2/g; 4.12×10^{-2} cm^3/g) while critically avoiding the severe particle agglomeration that plagues the latter; scanning electron microscopy unambiguously reveals that OBDC ash particles adhere to the internal pore walls and convoluted surfaces of the orange peel-derived carbon matrix, generating a rough, high-relief topography that multiplies available adsorption sites and maximizes solid–solution interfacial contact area between the passivator and the soil matrix, thereby enabling efficient physical sieving and entrapment of both dissolved metal cations and colloidal microbial cells within the hierarchical pore network, which spans micropores (<2 nm), mesopores, and macropores inherited from the orange peel template. Upon incorporation into the Cu–Pb co-

contaminated soil—spiked to nominal concentrations of 800 mg/kg Cu(II) and 1000 mg/kg Pb(II), approximately fourfold the Chinese GB 15618-2018 agricultural soil thresholds—the composite immediately deploys its surface chemistry arsenal, as Fourier-transform infrared spectroscopy confirms the retention of intense vibrational signatures at 3430 cm^{-1} (O–H stretching of surface hydroxyl groups), 2928 cm^{-1} (aliphatic C–H), 1608 cm^{-1} (carbonyl C=O), 1434 cm^{-1} (carboxyl –COOH), and 1100 cm^{-1} (sulfate/silicate moieties), all of which participate in ligand-exchange reactions wherein deprotonated –OH and –COOH groups coordinate directly with Cu^{2+} and Pb^{2+} to form stable inner-sphere surface complexes that effectively remove these cations from the soil solution; X-ray diffraction further identifies that OBDCs-OB preserves the crystalline mineralogy of the parent drilling cuttings, comprising quartz (SiO_2), calcite ($CaCO_3$), pyrite (FeS_2), muscovite ($KAl_2(AlSi_3O_{10})(OH)_2$), and kaolinite ($Al_2Si_2O_5(OH)_4$), minerals that collectively unlock additional immobilization pathways, chief among them cation exchange at the interlayer sites of sheet silicates, where loosely held Na^+, K^+, and Ca^{2+} ions are displaced by heavy-metal cations, a process directly quantified by the 18.29 cmol/kg elevation in cation exchange capacity (CEC) relative to untreated control soil, representing the largest CEC gain among all treatments including single-component OB and OBDC biochars. Concurrently, calcite and subsidiary carbonate phases embedded within the composite act as a sustained-release alkalinity reservoir, partially dissolving under the mild acidifying pressure exerted by heterotrophic microbial metabolism—which generates organic acids during glucose-driven growth—to liberate carbonate and bicarbonate anions that hydrolyze in soil moisture to yield hydroxide ions ($CO_3^{2-} + H_2O \rightleftharpoons HCO_3^- + OH^-$), thereby buffering the soil pH at 6.80±0.1 throughout the entire 83-day incubation period and preventing the pH from collapsing to the sub-6.0 values observed in treatments lacking carbonate-bearing amendments; this pH buffering is not merely a secondary benefit but a central mechanistic pillar because the maintained circumneutral pH actively promotes the precipitation of Cu(II) and Pb(II) as insoluble hydroxide and carbonate solids, a pathway that hard–soft acid–base (HSAB) theory rigorously explains as being disproportionately favorable for Pb(II)—classified as a hard Lewis acid—which forms exceptionally strong coordination bonds with hard Lewis bases such as surface hydroxyl groups, carbonate, and oxide ligands, whereas Cu^{2+} (a borderline/soft acid) engages in comparatively weaker interactions with these hard bases, thus accounting for the experimentally observed disparity wherein TCLP leaching toxicity of Pb is suppressed by 92.8% against 52.8% for Cu, and BCR acid-soluble fractions contract by 20.07% for Pb versus 18.21% for Cu, confirming that lead is driven more completely into stable residual and carbonate-bound pools. Beyond these abiotic immobilization routes, OBDCs-OB functions as a biocompatible platform that systematically rescues and stimulates the indigenous soil microbial consortium, which itself becomes an active participant in metal stabilization; the composite's porous architecture and buffered pH create a protective microenvironment that attenuates acute metal toxicity—particularly important given that Cu and Pb at the tested concentrations are bacteriostatic—allowing total bacterial counts to surge to a maximum of 8.6×10^{10} cfu/g on day 28, markedly outpacing treatments receiving only orange peel biochar or drilling-cuttings biochar, while dehydrogenase activity (a proxy for overall microbial respiratory vigor) peaks at 127.10 μg·TPE/(g·6h) and urease activity at 167.10 mg·NH_3-N/(kg·24h), both on day 28, reflecting intense metabolic turnover that drives the secretion of extracellular polymeric substances (EPS), siderophores, and organophosphate metabolites, all of which possess additional metal-chelating functional groups that bind residual mobile Cu^{2+} and Pb^{2+} into organo-metallic complexes, further depleting the acid-soluble metal pool and enriching reducible, oxidizable, and residual BCR fractions; 16S rDNA amplicon sequencing at 97% sequence similarity yields 10,593 operational taxonomic units and demonstrates that OBDCs-OB consistently produces the highest α-diversity (Shannon index: 8.69 on day 21; 2.26 on day 83) and richness (Chao1: 1658.06; ACE: 1683.64) across all treatments, selectively enriching heavy-metal-tolerant phyla—Proteobacteria, Actinobacteria, Firmicutes, and Acidobacteria—that are well-documented residents of contaminated soils, without disrupting the core phylum-level community structure, meaning that the composite enhances biodiversity as a whole while preserving ecological continuity and functional redundancy. In synthesis, the mechanistic architecture of OBDCs-OB remediation is neither linear nor reducible to a single interaction but rather constitutes a positive-feedback loop wherein waste-derived mineral phases (clay, carbonate, quartz) establish the physicochemical framework for instantaneous metal capture through ion exchange, complexation, and precipitation, the biochar scaffold prevents particle agglomeration and sustains high interfacial area while furnishing biocompatible habitat, the buffered pH maintains conditions permissive for robust microbial colonization and enzymatic activity, and the stimulated microbiome in turn secretes biopolymers and metabolites that achieve tertiary, biologically mediated metal locking into geochemically stable residual fractions, such that after 83 days the acid-soluble Cu and Pb pools are diminished by 18.21% and 20.07%, leaching toxicity is curtailed by 52.8% and 92.8%, CEC is augmented by 18.29 cmol/kg,

and soil microbial diversity and abundance are simultaneously maximized, collectively validating pyrolytic OBDCs-OB as a resource-circular, low-cost, and mechanistically robust strategy for the in-situ passivation and remediation of copper–lead co-contaminated soils that transcends the limitations of conventional single-mechanism amendments.

Table 1 Microbial community sequencing results

Sample	Valid sequences (No.)	Average length (bp)	OTUs (No.)	Shannon index	Chao1 index	ACE index	Coverage/%
Blank	38171	416	1064	4.29	1189.50	1257.01	99.2
C0 (21 d)	47066	423	1334	7.72	1445.47	1463.44	99.3
C1 (21 d)	44057	416	1361	8.17	1445.52	1442.70	99.3
C2 (21 d)	69657	414	1444	8.48	1535.78	1572.75	99.5
C3 (21 d)	46444	416	1404	8.44	1505.81	1501.68	99.4
C4 (21 d)	49950	415	1534	8.69	1658.06	1683.64	99.2
C0 (83 d)	43677	418	405	1.01	621.54	629.08	99.4
C1 (83 d)	57863	427	415	1.91	703.94	745.82	99.3
C2 (83 d)	65403	425	534	2.30	1000.96	985.02	99.2
C3 (83 d)	61164	419	510	2.12	769.17	882.44	99.1
C4 (83 d)	66442	421	588	2.26	1044.14	1068.43	99.3

Note: Valid sequences: number of effective sequences obtained from each soil sample. Average length: average length of effective sequences. OTUs: operational taxonomic units clustered at 97% sequence similarity. Shannon index: index for estimating species community diversity; higher values indicate greater community diversity. Chao1 and ACE indices: indices for estimating species community richness; higher values indicate greater community richness. Coverage: percentage of analyzed data in total sequences. OTU clustering was performed using Uparse software (V7.0.1090); Shannon index, Chao1, and ACE indices were calculated using Qiime software (V1.9.1).

4 Conclusion

Pyrolytic OBDCs-OB, endowed with –OH/–COOH groups, carbonate/clay minerals, and porous architecture, served as an effective adsorbent for Cu-Pb contaminated soil. Key findings: (1) CEC rose by 18.29 cmol/kg, surpassing single-component amendments; (2) pH was buffered at 6.80, with carbonate content dictating buffer strength; (3) acid-soluble Cu(II) and Pb(II) decreased 18.21% and 20.07%, leaching toxicity fell 52.8% and 92.8%, confirming robust passivation, especially for Pb; (4) microbial population and enzyme activities maximized at 8.6×10^{10} cfu/g, 127.10 μg·TPE/(g·6 h), and 167.10 mg·NH_3-N/(kg·24 h); (5) microbial diversity and richness expanded markedly, with dominant phyla unchanged, evidencing good biocompatibility. Pyrolytic OBDCs-OB thus represents a resource-efficient, low-cost strategy for remediating copper-lead co-contaminated soils.

References

[1] WANG H Y, HAN L, XIE D N, et al. Distribution characteristics of heavy metals in farmland soils around min ing areas and pollution assessment[J]. Environmental Science, 2022, 43(4): 2104-2114.

[2] HE J, XIE T J, YANG L H, et al. Effects of simulated acid rain on leaching characteristics of heavy metals and water-retaining capacity of soil in soil remediation[J]. Environmental Protection of Chemical Industry, 20 20, 40(4): 388-395.
[3] SUN N Y, QIU H Y, LAN G H, et al. Adsorption performance of Pb^{2+} by magnetic hydroxyapatite modified b oron nitride[J]. Fine Chemicals, 2022, 39(4): 725-733.
[4] LIU C. Experimental study on remediation of copper-lead contaminated soil by waste concrete PRB-electr okinetic combined method[D]. Jilin: Northeast Electric Power University, 2022.
[5] MA R S, CHEN J, XIA P, et al. Remediation of Cu(II), Pb(II) and Cr(III) contaminated soils with $CaCO_3$[J]. Jour nal of Northwest A&F University: Natural Science Edition, 2017, 45(1): 119-123, 30.
[6] ZHOU S K, TIAN L Y, RONG L S, et al. Remediation of uranium contaminated soil with three combined stabi lizers[J]. Fine Chemicals, 2020, 37(10): 2105-2111.
[7] TANG X C, CHEN J L, ZHANG M. Remediation effects of biochar on soil co-contaminated by copper, lead a nd cadmium[J]. Guangdong Agricultural Sciences, 2014, (12): 67-71.
[8] LU J K, WANG Z X, WU C Y, et al. Preparation and application of bentonite/sodium carboxymethyl cellulos e hydrogel[J]. Fine Chemicals, 2022, 39(7): 1376-1385.
[9] FU S B, MA Y, YUE C T. Research progress on harmless treatment and resource utilization of oil-based drill cuttings[J]. Applied Chemical Industry, 2021, 50(8): 2207-2214.
[10] HUANG Z Q, XU Z Y, QUAN Y H, et al. Effect evaluation of hammer-milling thermal desorption technology on oil-based drilling fluid cuttings[J]. Natural Gas Industry, 2018, 38(8): 83-90.
[11] YANG H, DIAO H L, ZHANG Y, et al. Treatment and novel resource-utilization methods for shale gas oil bas ed drill cuttings—A review[J]. Journal of Environmental Management, 2022, 317: 115462.
[12] LIU Y C, ZHOU S, LIU R, et al. Study on amino-directed modification of oil sludge-derived carbon and its ad sorption behavior of bisphenol A in water[J]. Separation and Purification Technology, 2022, 298: 121625.
[13] KUJAWSKA J, PAWLOWSKA M. The effect of amendment addition drill cuttings on heavy metals accumula tion in soils and plants: Experimental study and artificial network simulation[J]. J Hazard Mater, 2022, 425: 10.
[14] EL NAGGAR A, LEE M H, HUR J, et al. Biochar-induced metal immobilization and soil biogeochemical proce ss: An integrated mechanistic approach[J]. Science of the Total Environment, 2020, 698: 134112.
[15] CHO D W, YOON K, AHN Y, et al. Fabrication and environmental applications of multifunctional mixed met al-biochar composites (MMBC) from red mud and lignin wastes[J]. J Hazard Mater, 2019, 374: 412-419.
[16] YE X X, KANG S H, WANG H M, et al. Modified natural diatomite and its enhanced immobilization of lead, copper and cadmium in simulated contaminated soils[J]. J Hazard Mater, 2015, 289: 210-218.
[17] GAO Z L, XU Q X, LIU Y Q, et al. Biochar composite adsorbent for the removal of copper(II) and lead(II) fro m wastewater prepared by the pyrolysis of oil-based drilling cuttings and orange peels[J]. Analytical Lette rs, 2023, 56(17): 1-19.
[18] WU C, HUANG L, XUE S G, et al. Arsenic sorption by red mud-modified biochar produced from rice straw [J]. Environmental Science and Pollution Research, 2017, 24(22): 18168-18178.
[19] BAO H Y, WANG J F, ZHANG H, et al. Effects of biochar and organic substrates on biodegradation of polycy clic aromatic hydrocarbons and microbial community structure in PAHs-contaminated soils[J]. J Hazard M ater, 2020, 385: 121595.
[20] SCHAUMANN G E, KUNHI M Y. Considerations on cross-linking by bivalent cations in soil organic matter w ith low exchange capacity[J]. Journal of Plant Nutrition and Soil Science, 2018, 181(3): 441-452.
[21] GAO X L, ARTHUR C C T, WANG G, et al. Environmental status of Daya Bay surface sediments inferred fro m a sequential extraction technique[J]. Estuarine, Coastal and Shelf Science, 2010, 86(3): 369-378.
[22] CHEN C W, CHEN C F, HUNG C M, et al. Evaluating the leachable metals in Kaohsiung Harbor sediment usi ng the toxicity characteristic leaching procedure (TCLP)[J]. Desalination and Water Treatment, 2015, 54(4 /5): 1260-1269.
[23] JIA J L, ZONG S, HU L, et al. The dynamic change of microbial communities in crude oil-contaminated soils from oil fields in China[J]. Soil Sediment Contam, 2017, 26(2): 171-183.
[24] JIANG B, ADEBAYO A, JIA J L, et al. Impacts of heavy metals and soil properties at a Nigerian e-waste site o n soil microbial community[J]. J Hazard Mater, 2019, 362: 187-195.
[25] MENG X, HU R. Nitrogen/phosphorus enriched biochar with enhanced porosity activated by guanidine ph osphate for efficient passivation of Pb(II), Cu(II) and Cd(II)[J]. Journal of Molecular Liquids, 2021, 323: 115 071.

[26] LIANG X Y, LIANG T B, ZHOU F J, et al. Impact of shut-in time on production after hydraulic fracturing in fra ctured shale gas formation: An experimental study[J]. Journal of Natural Gas Science and Engineering, 202 1, 88: 103773.
[27] ZOLFAGHARI A, DEHGHANPOUR H, NOEL M, et al. Laboratory and field analysis of flowback water from ga s shales[J]. Journal of Unconventional Oil and Gas Resources, 2016, 14: 113-127.
[28] REES F, SIMONNOT M O, MOREL J L. Short-term effects of biochar on soil heavy metal mobility are contro lled by intra-particle diffusion and soil pH increase[J]. European Journal of Soil Science, 2014, 65(1): 149-1 61.
[29] BIN Z, CHEN J, SHAFI M, et al. Effect of lead (Pb) on antioxidation system and accumulation
[30] HARTMANN M, WIDMER F. Community structure analyses are more sensitive to differences in soil bacteri al communities than anonymous diversity indices[J]. Applied and Environmental Microbiology, 2006, 72(1 2): 7804-7812.
[31] RAHMAN Z, SINGH V P. Assessment of heavy metal contamination and Hg-resistant bacteria in surface wa ter from different regions of Delhi, India[J]. Saudi J Biol Sci, 2018, 25(8): 1687-1695.
[32] ZHAO X Q, HUANG J, LU J, et al. Study on the influence of soil microbial community on the long-term heav y metal pollution of different land use types and depth layers in mine[J]. Ecotox Environ Safe, 2019, 170: 2 18-226.
[33] ZHAO X Q, HUANG J, ZHU X Y, et al. Ecological effects of heavy metal pollution on soil microbial communit y structure and diversity on both sides of a river around a mining area[J]. International Journal of Environ mental Research and Public Health, 2020, 17(16): 218-226.
[34] AWASTHI S K, LIU T, AWASTHI M K, et al. Evaluation of biochar amendment on heavy metal resistant bact eria abundance in biosolids compost[J]. Bioresource Technology, 2020, 306: 123114.